BMC Cancer

RESEARCH

Open Access

Periprostatic fat magnetic resonance imaging based radiomics nomogram for predicting biochemical recurrence-free survival in patients with non-metastatic prostate cancer after radical prostatectomy

Xiao-Hui Wu[1,2†], Zhi-Bin Ke[1,2†], Ze-Jia Chen[1,2†], Wen-Qi Liu[1,2†], Yu-Ting Xue[1,2], Shao-Hao Chen[1,2], Dong-Ning Chen[1,2], Qing-Shui Zheng[1,2], Xue-Yi Xue[1,2,3], Yong Wei[1,2*] and Ning Xu[1,2,3*]

Abstract

Objective To build and validate a periprostatic fat magnetic resonance imaging (MRI) based radiomics nomogram for prediction of biochemical recurrence-free survival (bRFS) of patients with non-metastatic prostate cancer (PCa) receiving radical prostatectomy (RP).

Methods A retrospective study was conducted on 356 patients with non-metastatic PCa who underwent preoperative mpMRI followed by RP treatment at our institution. Radiomic features were extracted from both intratumoral region and the periprostatic fat region, which were segmented on images obtained through T2-weighted imaging (T2WI) and apparent-diffusion coefficient (ADC) imaging. Three radiomics models were developed by applying the Least absolute shrinkage and selection operator (LASSO) Cox regression, followed by Cox risk regression to construct a combined radiomics-clinical model by integrating the optimal radiomics score and clinicopathological risk factors to draw a nomogram. The predictive performance was evaluated using receiver operating characteristic (ROC) curves, Kaplan-Meier analysis and calibration curves.

Results One hundred and twenty-one patients (33.98%) experienced biochemical recurrence. ROC analyses showed that the Area Under the Curve (AUC) of the periprostatic fat-intratumoral radiomics model demonstrated the highest AUC at 0.921 (95%CI, 0.857–0.981), 0.875 (95%CI, 0.763–0.950), 0.854 (95%CI, 0.706–0.923) for 1-year, 3-years and 5-years bRFS. Multivariate Cox regression analysis revealed that Pathological T stage, ISUP grading group and Positive surgical margin were independent prognostic factors for predicting bRFS. A radiomics-clinical nomogram based on these clinical predictors and periprostatic fat-intratumoral radiomics score was constructed. Kaplan-Meier analyses showed that radiomics-clinical nomogram was significantly related with survival of PCa ($P < 0.001$); and calibration

†Xiao-Hui Wu, Zhi-Bin Ke, Ze-Jia Chen and Wen-Qi Liu contributed equally to this work.

*Correspondence:
Yong Wei
weiyong2017@fjmu.edu.cn
Ning Xu
drxun@fjmu.edu.cn
Full list of author information is available at the end of the article

curves revealed the predicted and observed survival probability of 1-year, 3-year and 5-year bRFS had high degree of consistency in the training and validation group. The radiomics-clinical nomogram showed a significant improvement than the clinical model for 1-year (AUC, 0.944; 95%CI, 0.912–0.990 vs. AUC, 0.839; 95%CI, 0.661–0.928; $P=0.009$), 3-year (AUC, 0.864; 95%CI, 0.772–0.969 vs. AUC, 0.776; 95%CI, 0.602–0.872; $P=0.008$), and 5-year bRFS (AUC, 0.907; 95%CI, 0.836–0.982 vs. AUC, 0.819; 95%CI, 0.687–0.915; $P=0.027$).

Conclusions This study developed and validated the radiomics-clinical nomogram for the prediction of bRFS in non-metastatic PCa patients underwent RP.

Keywords Prostate cancer, Radiomics, Periprostatic fat, Biochemical recurrence-free survival, Nomogram

Introduction

Prostate cancer (PCa) is globally recognized as one of the most prevalent malignancies of the genitourinary system in males, with its morbidity in men rising to second place, being the sixth leading cause of death [1]. Radical prostatectomy (RP) is regarded as the primary treatment option for non-metastatic PCa [2]. Nevertheless, studies have shown that approximately 27–53% of patients receiving RP experienced biochemical recurrence (BCR) [3]. Patients who experience BCR are at an increased likelihood of developing clinical metastases and facing a higher risk of poor prognosis [4]. Therefore, it is crucial to accurately recognize BCR for subsequent decision-making regarding PCa patients.

Radiomics is an extensively studied method in various tumors, involving the extraction of quantitative features from images to estimate clinical events [5, 6]. Previous researches have demonstrated the great value of radiomic features obtained from multiparametric magnetic resonance imaging (mpMRI) in PCa detection, Gleason Score discrimination, and treatment response assessment [7, 8]. Woźnicki et al. [9]. found that ensemble models combining radiomics, Prostate Imaging-Reporting and Data System, prostate-specific antigen density, and digital rectal examination outperformed experienced radiologist assessments for PCa characterization and clinically significant PCa detection. Wang et al. [10]. revealed that mpMRI radiomics features were crucial for predicting bone metastases in PCa patients, and combining clinical characteristics with MRI-based radiomics features could significantly enhance the accuracy of prediction [10].

Previous radiomics studies of PCa have primarily concentrated on the intratumoral region [9–12], leaving the role of radiomics features derived from periprostatic fat tissue relatively unexplored. The prostate gland is surrounded by periprostatic fat tissue, and several studies have shown the tight relationship between periprostatic fat and PCa progression [13–15]. A series of metabolic changes and bidirectional crosstalk of many molecules exist between tumor cells and adipocytes [16]. It has been reported that pro-inflammatory adipokines, tumor necrosis factor (TNF)-α, and C-C motif chemokine ligand 7 (CCL7) secreted by periprostatic fat tissue can promote PCa cell proliferation, migration, and invasion. Coy et al. [17]. discovered that patients with high-risk PCa exhibited alterations in the lipid composition of periprostatic fat, which influenced tumor cell processes by affecting PCa cell lipid metabolism. The interactions between PCa cells and periprostatic fat cells can induce phenotypical changes in adipose tissue, which can manifest as subtle alterations on MRI that may not be discernible to the naked eye. These alterations may contain key features associated with the drug resistance, and progress of the disease.

However, to our knowledge, there was no study exploring the correlation between MRI radiomics features derived from periprostatic fat region and the BCR or biochemical recurrence-free survival (bRFS) of PCa patients receiving RP treatment. Therefore, this study retrospectively collected clinical information and MRI imaging data from 356 PCa patients receiving RP treatment, and extracted radiomics features from periprostatic fat and intratumoral region to assess the value of periprostatic fat radiomics features in predicting bRFS.

Materials and methods

Patients and data collection

This study was approved by the Ethics Committee of the First Affiliated Hospital of Fujian Medical University and written informed consent was provided by all patients. We conducted a retrospective analysis of 356 non-metastatic PCa patients who underwent pre-operative prostate mpMRI and RP in the First Affiliated Hospital of Fujian Medical University between January 2013 and August 2020. Tumors were staged following the American Joint Committee on Cancer/ Union for International Cancer Control (AJCC/UICC) Tumor, Node, Metastasis (TNM) classification system 2017 Edition. The absence of distant metastasis was confirmed through pre-treatment mpMRI, Computed Tomography (CT), bone scanning, or Prostate-specific membrane antigen ligand positron emission tomography/CT (PSMA PET/CT).

The inclusion criteria were as follows: (1) pathologically diagnosed with PCa; (2) prostate mpMRI was performed

before RP. The exclusion criteria were as follows: (1) were without T2 weighted images (T2WI) or Apparent Diffusion Coefficient (ADC) images [$n=63$]; (2) received prior additional therapies (radiotherapy, chemotherapy, endocrine) before RP [$n=126$]; (3) were with prostate specific antigen (PSA) persistence[$n=28$]; (4) incomplete clinicopathologic data [$n=17$]; (5) MRI images were of insufficient quality [$n=34$]; (6) the follow up information did not include postoperative serum PSA measurements [$n=19$]. Eventually, a total of 356 non-metastatic PCa patients with complete clinicopathologic data were enrolled and randomly divided into training/validation sets at a ratio of 7:3 (treated between 2013 and 2016; 118 cases in the training group and 53 cases in the validation group, respectively), and testing group (treated between 2017 and 2020; $n=185$). The comparison of clinicopathological characteristics between included and excluded patients is shown in Supplementary Table 1.

The clinicopathological date of patients were collected for analysis, including age, body mass index (BMI), International Society of Urological Pathology (ISUP) Gleason grading group, pathological T stage, initial Prostate-specific antigen (PSA) at diagnosis, lymph nodes metastasis, peri-prostatic fat involvement, perineal invasion, lymphovascular invasion and positive surgical margin.

Definition of biochemical recurrence, post-operative PSA follow-up protocol

According to the European Association of Urology (EAU) Guidelines of 2021 edition, BCR is determined by the presence of two consecutive serum prostate-specific antigen (PSA) measurements exceeding 0.2 ng/mL, bRFS refers to the period between the date of RP and the point of BCR. Undetectable PSA is defined as a serum PSA level of less than 0.1 ng/mL within 4 to 8 weeks of surgery [18]. Patients underwent serum PSA testing at 6–8 weeks post-surgery, followed by every 3 months for the first year, every 6 months for the second year, and annually thereafter. Routine follow-up for patients was conducted through various means, including In-person visits, telephone communication.

Examination procedure of mpMRI

All patients were imaged on 3 Tesla (3T) MRI scanners (Siemens Healthcare, Erlangen, Germany, Verio 3.0T) with pelvic phased-array coil within two weeks before RP. A supine position was adopted for the patient, and a comprehensive scan of the entire prostate was executed with the scanning range centered on the central part of the prostate. The patient was asked to have a bowel movement before the examination and ensure moderate bladder filling. The scanning sequences included transverse, sagittal, and frontal T2WI images, diffusion-weighted imaging (DWI) images, and corresponding ADC maps. The detailed mpMRI sequences parameters were presented in Supplementary Table 2. The gadopentetate dimeglumine (Gd-DTPA) was administered via a pressure injector into the dorsal hand vein at a flow rate of 3 mL/s. A total of 18 sequential scans were performed, with each individual scan lasting for 11 s.

Delineation of regions of interest

Two experienced radiologists with more than 8 years of expertise in prostate mpMRI interpretation, blinded to each other's delineations and clinical data, independently outlined the regions of interest (ROI) for intratumoral and periprostatic fat areas in T2WI and ADC images using ITK-SNAP software version 3.6.0. (Yushkevich P and Gerig G). The periprostatic fat region includes the neurovascular bundles, where the seminal vesicle and metastatic lymph nodes excluded. The intratumoral and periprostatic fat ROI were showed in Supplementary Fig. 1 and Supplementary Fig. 2. To select robust features, fifty patients were randomly selected to conduct a test-retest study. The inter-observer repeatability of the extracted features between two radiologists was assessed, and the intra-observer repeatability was assessed by comparing the extracted features of the same radiologist (twice, one week apart).

Radiomics features extraction and selection

Radiomics features were extracted using Python (version 3.7.3) package PyRadiomics version 3.0. Radiomic features were extracted from original images as well as two basic image filters, namely wavelet and Laplacian of Gaussian (LoG) images. The extracted features included: (1) shape features; (2) first-order statistical features; (3) gray-level run length matrix (GLRLM) features; (4) gray-level co-occurrence matrix (GLCM) features; (5) gray-level dependence matrix (GLDM) features; (6) gray-level size zone matrix (GLSZM) features; (7) neighboring gray tone difference matrix (NGTDM) features.

To remove scale variations and ensure comparability, all features underwent normalization using the Z-Score transform. Afterward, characteristics displaying limited repeatability were eliminated from subsequent examination. Inter-observer and intra-observer repeatability were quantified by employing the infraclass correlation coefficient (ICC). Features with ICC greater than 0.8 were chosen for further analysis. In order to select the features with the highest correlation and minimum redundancy, radiomics features from intratumoral and periprostatic fat ROIs were ranked by using the maximum relevance minimum redundancy (mRMR) algorithm respectively.

Radiomics scores, clinical model, nomogram construction and validation

In the training group, the Least absolute shrinkage and selection operator (LASSO) Cox regression was used to determine three radiomics scores based on the selected radiomics features: (1) periprostatic fat radiomics score; (2) intratumoral radiomics score; (3) combined periprostatic fat-intratumoral radiomics score. The radiomics score with the highest area under the receiver operating characteristic (ROC) was selected for further exploration. Significant clinical features were selected through univariable and multivariable Cox risk regression analyses for clinical model building. And the combined radiomics-clinical model was constructed with both significant clinical parameters and optimal radiomics score using multivariable Cox risk regression analysis. Finally, according to the combined radiomics-clinical model, the nomogram for predicting bRFS was constructed to achieve a more intuitive purpose of predicting survival.

Kaplan-Meier analysis was conducted to assess the survival prediction performance of the radiomics scores, clinical model, and nomogram in both the training and validation groups. ROC curves were plotted to evaluate the diagnostic performance of these models. Additionally, calibration curves were generated to evaluate the calibration performance of the nomogram.

Statistical analysis

Statistical analyses were conducted using SPSS version 26 (IBM SPSS, Inc., Armonk, NY), and R software (R Foundation for Statistical Computing, Vienna, Austria version 4.1.0). Categorical variables were compared using the chi-square test or Fisher's exact test, while continuous variables were assessed using the independent t-test or Mann-Whitney U test. The ICC was calculated with R package "psych". The mRMR analysis was carried out by the "mRMRe" package. The LASSO Cox regression was conducted with R package "glmnet"; Univariable and multivariable Cox regression analyses, as well as Kaplan-Meier analysis, were conducted using the "survival" and "survminer" packages.; Calculating the AUC (95% confidence interval (CI)) and comparing different ROC curves were performed by R package "timeROC". Nomograms and calibration curves were created using the "rms" and "survival" packages. A two-sided P value < 0.05 was considered statistically significant.

Results

Baseline characteristics

The flow diagram of this study is presented in Fig. 1. The baseline clinical characteristics information of 356 non-metastatic PCa patients were listed in Table 1. The mean (standard deviation (SD)) age of all patients was 69.19 (6.46) years. The Initial PSA at diagnosis of all patients was 21.57 (6.20–97.04) ng/ml. The number of patients with ISUP group ≤ 3 was 194 (54.49%), and the number of patients with ISUP group > 3 was 162 (45.51%). There were no significant differences observed in Age, BMI, initial PSA level, ISUP grading group, Lymph nodes metastasis, Positive surgical margin, Peri-prostatic fat involvement, Perineal invasion, Lymphovascular invasion as well as BCR rates between the training group, validation group, and testing group.

The median follow-up duration in the study was 51.07 months, ranging from 46.48 to 55.67 months. The number of patients who experienced BCR was 121 (33.98%). During the follow-up of the 121 patients who experienced BCR, eleven (9.09%) patients developed local recurrences. Of these, eight patients received salvage radiotherapy, and 3 patient received salvage radiotherapy combined with androgen deprivation therapy (ADT) (leuprorelin, 3.75 mg every four weeks). Additionally, fifteen (12.40%) patients developed distant metastases. Of these, ten patients were treated with ADT combined with abiraterone acetate (1000 mg daily) plus prednisone (5 mg daily) or enzalutamide (160 mg daily), and 5 patients were treated with ADT combined with chemotherapy (docetaxel, dose of 75 mg/sqm every three weeks, six cycles).

Identification of periprostatic fat and intratumoral radiomics feature

We extracted 2632 radiomics features form the periprostatic fat ROI (1316 radiomics features from ADC and 1316 radiomics features from T2WI) and intratumoral ROI (1316 radiomics features from ADC and 1316 radiomics features from T2WI), respectively. After ICC analysis, the count of periprostatic fat features decreased to 1937 (899 features from ADC and 1038 features from T2WI), while the count of intratumoral features decreased to 1831 (932 features from ADC and 899 features from T2WI). The remaining features were ranked by the mRMR algorithm to retain the top 40 periprostatic fat and intratumoral radiomics features for the construction of radiomic scores (Supplementary Table 3).

Construction and validation of radiomics

By employing LASSO Cox regression analysis, we identified eight radiomics features for constructing the periprostatic fat radiomics score, six features for constructing the intratumoral radiomics score, and another eight features for constructing the periprostatic fat-intratumoral radiomics score (Table 2; Fig. 2). The formula for the radiomics scores was as following.

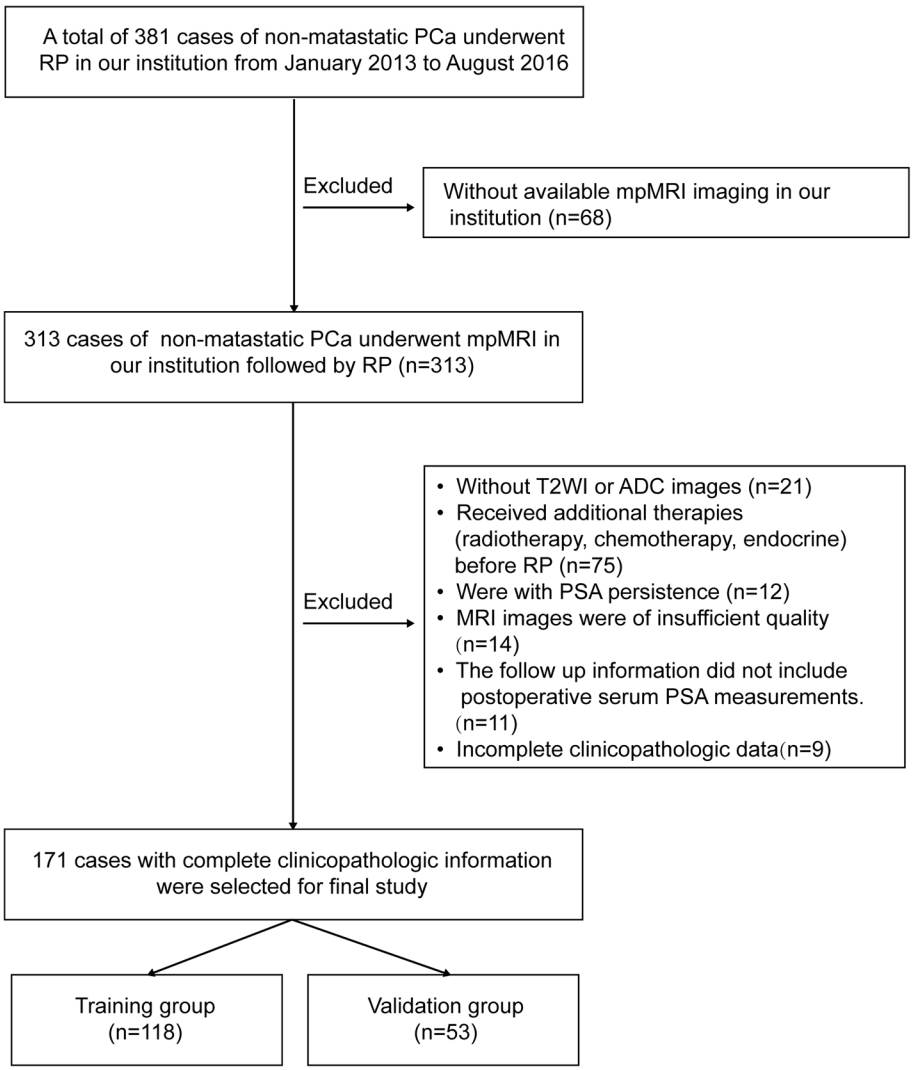

Fig. 1 Flow diagram of this study

$$\text{Radiomics score} = \sum_{i=1}^{n} (\text{Radiomics feature}_i * \text{Coef}_i)$$

The risk score of each patient was calculated based on radiomics scores. All patients were classified into high-risk and low-risk groups according to the median risk score. Kaplan-Meier analysis conducted in training and validation groups were illustrated in Fig. 3. Survival analysis demonstrated that the bRFS of patients with high-risk was significantly decreased compared with that of patients with low-risk.

The ROC curves of the three models in the training and validation groups were shown in Fig. 4. The AUCs of the periprostatic fat radiomics model in the training group were 0.901 (95%CI, 0.817–0.982), 0.856 (95%CI, 0.741–0.923), 0.833 (95%CI, 0.687–0.921) at 1-year, 3-years and 5-years bRFS in training cohort (Fig. 4A), and the AUCs in the validation group were 0.823 (95%CI, 0.663–0.965), 0.796 (95%CI, 0.656–0.943), 0.771 (95%CI, 0.642–0.905) at 1-year, 3-years and 5-years bRFS (Fig. 4B). The AUCs of the intratumoral radiomics model in the training group were 0.803 (95%CI, 0.640–0.889), 0.778 (95%CI, 0.606–0.865), 0.758 (95%CI, 0.600–0.827) at 1-year, 3-years and 5-years (Fig. 4C), and the AUCs in the validation group were 0.858 (0.731–0.961), 0.754 (95%CI, 0.624–0.895), 0.702 (95%CI, 0.610–0.863) at 1-year, 3-years and 5-years (Fig. 4D). The AUCs of the periprostatic fat-intratumoral radiomics model in the training group were 0.921 (95%CI, 0.857–0.981), 0.875 (95%CI, 0.763–0.950), 0.854 (95%CI, 0.706–0.923) at 1-year, 3-years and 5-years (Fig. 4E), and the AUCs in the validation group were 0.858 (95%CI, 0.731–0.961), 0.754

Table 1 Baseline characteristics of 356 PCa patients

Patient Characteristics	Training group ($n=118$)	Validation group ($n=53$)	Testing group ($n=185$)	*P* value
Age at diagnosis (years)	68.53 ± 5.93	68.36 ± 6.44	69.87 ± 6.76	0.868[a]/0.078[b]/0.148[c]
BMI (kg/m2)	23.86 ± 2.69	23.06 ± 2.62	23.83 ± 4.01	0.071[a]/0.962[b]/0.185[c]
Initial PSA at diagnosis (ng/ml)	21.24 (8.09–97.04)	20.86 (6.20–48.87)	21.43 (6.46–54.67)	0.412[a]/0.074[b]/0.616[c]
Pathological T stage				0.001[a]/0.001[b]/0.291[c]
≤ pT2c	81 (68.64%)	22 (41.51%)	92 (49.72%)	
≥ pT3	37 (31.36%)	31 (58.49%)	93 (50.27%)	
ISUP grading group of surgical specimens				0.872[a]/0.766[b]/0.957[c]
≤ 3	63 (53.39%)	29 (54.72%)	102 (55.13%)	
>3	55 (46.61%)	24 (45.28%)	83 (44.97%)	
Lymph nodes metastasis				0.281[a]/0.603[b]/0.109[c]
Yes	13 (11.00%)	9 (17.00%)	17 (9.21%)	
No	105 (89.00%)	44 (83.00%)	168 (90.89%)	
Positive surgical margin				0.775[a]/0.486[b]/0.410[c]
Yes	45 (38.14%)	19 (35.85%)	78 (42.17%)	
No	73 (61.87%)	34 (64.15%)	107 (53.83%)	
Peri-prostatic fat involvement				0.646[a]/0.726[b]/0.850[c]
Yes	3 (2.54%)	2 (3.77%)	6 (3.25%)	
No	115 (97.46%)	51 (96.23%)	179 (96.75%)	
Perineal invasion				0.981[a]/0.677[b]/0.773[c]
Yes	11 (9.32%)	5 (9.43%)	20 (11.85%)	
No	107 (90.68%)	48 (90.57%)	165 (89.15%)	
Lymphovascular invasion				0.686[a]/0.704[b]/0.484[c]
Yes	16 (13.56%)	6 (11.32%)	27 (15.13%)	
No	102 (86.44%)	47 (88.68%)	158 (84.86%)	
Biochemical recurrence				0.160[a]/0.521[b]/0.318[c]
Yes	36 (30.51%)	22 (41.51%)	63 (34.05%)	
No	82 (69.49%)	31 (58.49%)	122 (65.95%)	
Median Follow-up (months)	52.01 (44.61–59.41)	53 (47.07–59.22)	49.44 (44.16–54.84)	

PCa Prostate cancer, *BMI* Body mass index, *PSA* Prostate-specific antigen, *ISUP* International Society of Urological Pathology

[a] Training group vs. Validation group

[b] Training group vs. Testing group

[c] Validation group vs. Testing group

(95%CI, 0.624–0.895), 0.702 (95%CI, 0.610–0.863) for 1-year, 3-years and 5-years bRFS (Fig. 4F).

The performance of each radiomics score was compared and summarized in Table 3. The periprostatic fat-intratumoral radiomics score achieved the highest AUC values for 1-year (AUC: 0.921, 95% CI: 0.857–0.981), 3-year (AUC: 0.875, 95% CI: 0.763–0.950), and 5-year (AUC: 0.854, 95% CI: 0.706–0.923) bRFS. The periprostatic fat-intratumoral radiomics score showed a significant improvement in predicting 1-year (AUC: 0.803; 95%CI: 0.640–0.889; $P=0.010$) and 3-year bRFS (AUC: 0.778; 95%CI: 0.606–0.865; $P=0.017$) compared to the intratumoral radiomics score. Whereas periprostatic fat radiomics model and intratumoral radiomics model demonstrated similar performance for 1-year (AUC: 0.901, 95% CI: 0.817–0.982; $P=0.051$), 3-year (AUC: 0.856, 95% CI: 0.741–0.923; $P=0.136$), and 5-year (AUC: 0.833, 95% CI: 0.687–0.921; $P=0.241$) bRFS. Therefore, the periprostatic fat-intratumoral radiomics model was identified for further analysis.

Construction and validation of clinical model

Univariable Cox regression analysis revealed that initial PSA at diagnosis ($P=0.05$; HR = 1.024; 95%CI, 1.007–1.042), pathological T stage ($P=0.002$; HR = 2.780; 95%CI, 1.438–5.374), ISUP grading group of surgical specimens ($P<0.001$; HR = 3.466; 95%CI, 1.699–7.069), positive surgical margin ($P<0.001$; HR = 4.401; 95%CI, 2.215–8.744) were associated with bRFS of PCa patients receiving RP treatment (Table 4). A clinical model was constructed using multivariate Cox regression analysis based on the results obtained from univariable Cox regression analysis (Fig. 5A).

Table 2 LASSO COX regression analyses constructing three radiomics scores for predicting bRFS in patient with non-metastatic PCa receiving RP treatment

ROIs	MRI sequences	Group and filters	Feature class	Feature	Coef
Periprostatic fat radiomics features					
Periprostatic fat	ADC	Wavelet (HLL)	GLSZM	Large Area High Gray Level Emphasis	0.349
	T2WI	Wavelet (HLL)	NGTDM	Contrast	−2.132
	ADC	Wavelet (HHH)	GLSZM	Small Area Emphasis	0.661
	T2WI	Original	Shape	Major Axis Length	0.839
	ADC	LoG (sigma = 3.0.mm 3D)	GLCM	Sum Squares	2.613
	ADC	Wavelet (HHH)	GLCM	Idn	1.160
	T2WI	Wavelet (LHH)	GLSZM	Zone Variance	0.777
	T2WI	Wavelet (HLH)	GLSZM	Large Area Emphasis	−0.343
Intratumoral radiomics features					
Intratumoral region	ADC	wavelet (LHH)	First order	Interquartile Range	0.837
	ADC	Wavelet (HLL)	First order	Skewness	0.000
	ADC	Wavelet (HHL)	GLCM	Joint Energy	0.328
	ADC	LoG (sigma = 5.0.mm 3D)	GLRLM	Run Length Non Uniformity Normalized	0.183
	ADC	LoG (sigma = 2.0.mm 3D)	GLCM	Sum Entropy	0.180
	T2WI	Wavelet (LLL)	GLCM	Idn	−0.002
Periprostatic fat-intratumoral radiomics features					
Periprostatic fat	T2WI	Wavelet (HLL)	NGTDM	Contrast	−0.708
Periprostatic fat	ADC	wavelet (HHH)	GLSZM	Small Area Emphasis	0.215
Periprostatic fat	T2WI	Original	Shape	Major Axis Length	0.327
Periprostatic fat	ADC	LoG (sigma = 3.0.mm 3D)	GLCM	Sum Squares	0.869
Periprostatic fat	T2WI	Wavelet (LHH)	GLSZM	Zone Variance	0.072
Intratumoral region	ADC	Wavelet (LHH)	First order	Interquartile Range	0.713
Intratumoral region	ADC	LoG (sigma = 5.0.mm 3D)	GLRLM	Run Length Non Uniformity Normalized	0.448
Intratumoral region	ADC	LoG (sigma = 3.0.mm 3D)	GLCM	Imc2	0.035

LASSO The Least absolute shrinkage and selection operator, *bRFS* biochemical recurrence-free survival, *PCa* Prostate cancer, *RP* radical prostatectomy, *ROIs* Regions of interests, *MRI* Magnetic resonance imaging, *Coef* Coefficient, *ADC* Apparent-diffusion coefficient, *T2WI* T2-weighted imaging, *GLSZM* Gray-level size zone matrix, *NGTDM* neighboring gray tone difference matrix, *GLCM* Gray-level co-occurrence matrix, *GLRLM* Gray-level run length matrix, *LoG* Laplacian of Gaussian

The risk score of each patient was calculated based on the clinical risk scores. All patients were categorized into high-risk and low-risk groups according to the median risk score. As illustrated in Fig. 5B and E. Kaplan-Meier analysis revealed that patients with a high-risk profile experienced significantly shorter bRFS in comparison to those in the low-risk group ($P < 0.001$), with an AUC of 0.839, 0.776, and 0.819 for 1-year, 3-year, and 5-year bRFS, respectively, in the training group. And in the validation group, high-risk patients had significantly shorter bRFS than low-risk patients ($P = 0.007$), with an AUC of 0.838, 0.761, and 0.810 for 1-year, 3-year, and 5-year bRFS, respectively.

Development and validation of combined radiomics-clinical nomogram

Based on the periprostatic fat-intratumoral radiomics score and significant clinical characteristics, a combined radiomics-clinical nomogram for predicting bRFS of PCa patients was developed by using multivariate Cox regression analysis (Fig. 6). The AUCs of radiomics-clinical nomogram in the training group were 0.944 (95%CI, 0.912–0.990), 0.864 (95%CI, 0.772–0.969), 0.907 (95%CI, 0.836–0.982) at 1-year, 3-years and 5-years bRFS in training cohort (Fig. 7A), the AUCs in the validation group were 0.875 (95%CI, 0.750–0.998), 0.814 (95%CI, 0.676–0.953), 0.869 (95%CI, 0.712–0.997) at 1-year, 3-years and 5-years bRFS (Fig. 7C), and AUCs in the testing group were 0.815 (95%CI, 0.664–0.921), 0.729 (95%CI, 0.641–0.883), 0.854 (95%CI, 0.702–0.913) (Fig. 7E). Kaplan-Meier analysis revealed that patients with high-risk experienced significantly shorter bRFS in comparison to those in the low-risk group ($P < 0.001$) in the training group, validation group, and testing group (Fig. 7B, D and F). In addition, the calibration curves of the radiomics-clinical nomogram revealed that the predicted and observed survival probability of 1-years, 3-year and 5-year bRFS had high degree of consistency in the training group, validation group, and testing group (Fig. 8).

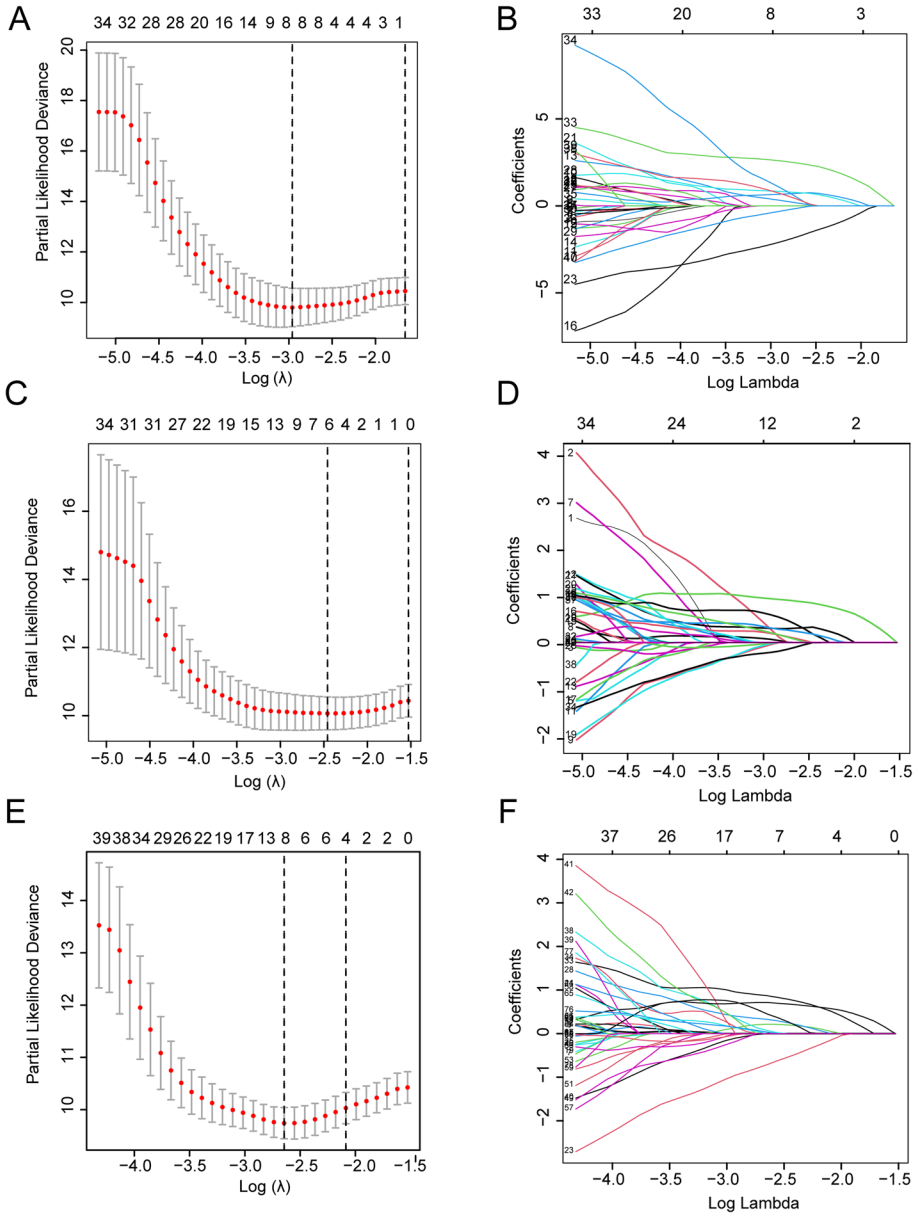

Fig. 2 LASSO Cox regression analyses of three radiomics models. **A**, **C**, **E** The partial likelihood deviance was plotted versus log (λ). The y-axis indicates the partial likelihood deviance, while the lower x-axis indicates the log (λ) and the upper x-axis represents the average number of predictors. Dotted vertical lines were drawn at the optimal values using the minimum criteria and 1 standard error of the minimum criteria. The tuning parameter (λ) was selected in the LASSO model via 10-fold cross-validation based on minimum criteria. **A** The lambda.min used in the LASSO algorithm for the periprostatic fat radiomics score is 0.05181153; **B** The lambda.min used in the LASSO algorithm for the intratumoral radiomics score is 0.08555169; **C** The lambda.min used in the LASSO algorithm for the periprostatic fat-intratumoral radiomics score is 0.07075123. The coefficients (y-axis) were plotted against log (lambda) and (**B**) 8 features with nonzero coefficients were selected to build periprostatic fat radiomics model, **D** 6 features with nonzero coefficients were selected to build intratumoral radiomics model, **F** and 8 features with nonzero coefficients were selected to build periprostatic fat-intratumoral radiomics model. LASSO, the Least absolute shrinkage and selection operator

The comparison of ROC curves for the optimal radiomics score, the clinical model, and the radiomics-clinical nomogram was presented in Table 5. The radiomics-clinical nomogram demonstrated the highest AUC values for 1-year bRFS (AUC: 0.944, 95%CI: 0.912–0.990) and 5-year bRFS (AUC: 0.907, 95%CI: 0.836–0.982) in the training group. Furthermore, the radiomics-clinical nomogram exhibited a substantial improvement compared to clinical model in predicting 1-year (AUC: 0.944; 95%CI, 0.912–0.990 vs. AUC:

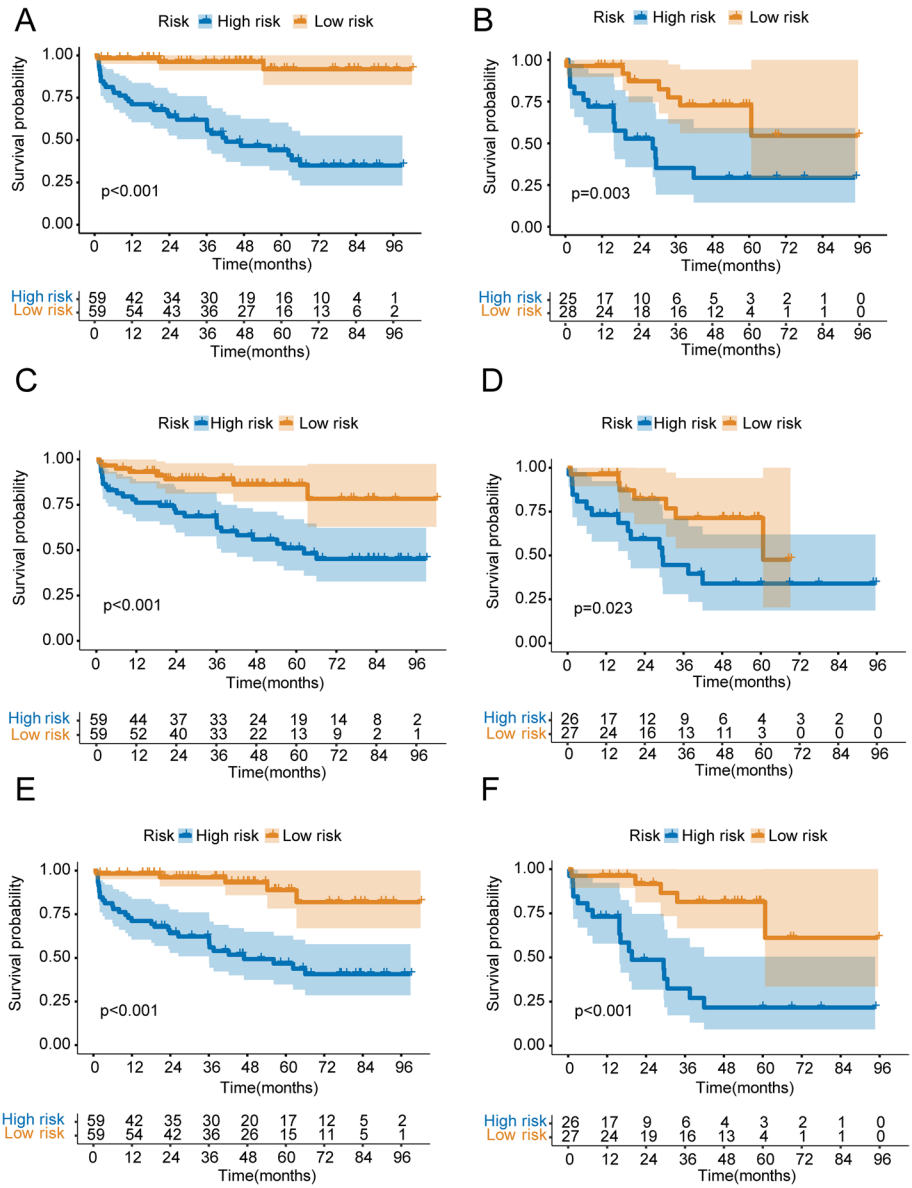

Fig. 3 Kaplan-Meier curve analyses of three radiomics models. **A** periprostatic fat radiomics model in the training group. **B** periprostatic fat radiomics model in the validation group. **C** intratumoral radiomics model in the training group. **D** intratumoral radiomics model in the validation group. I periprostatic fat-intratumoral radiomics model in the training group. **F** periprostatic fat-intratumoral radiomics model in the validation group

0.839; 95%CI, 0.661–0.928; $P=0.009$), 3-year (AUC: 0.864; 95%CI, 0.772–0.969 vs. AUC: 0.776; 95%CI, 0.602–0.872; $P=0.008$), and 5-year bRFS (AUC: 0.907; 95%CI, 0.836–0.982 vs. AUC: 0.819; 95%CI, 0.687–0.915; $P=0.027$) respectively. Additionally, no statistically significant disparity was observed between the performance of the periprostatic fat-intratumoral radiomics score and the clinical model.

Discussion

To our knowledge, the present study is the first to investigate the value of a nomogram constructed based on periprostatic fat radiomics in predicting the BFS in localized PCa patients after RP. Our findings revealed that the periprostatic fat radiomics score and intratumoral radiomics score exhibited comparable predictive ability for bRFS in PCa patients. However, upon combining

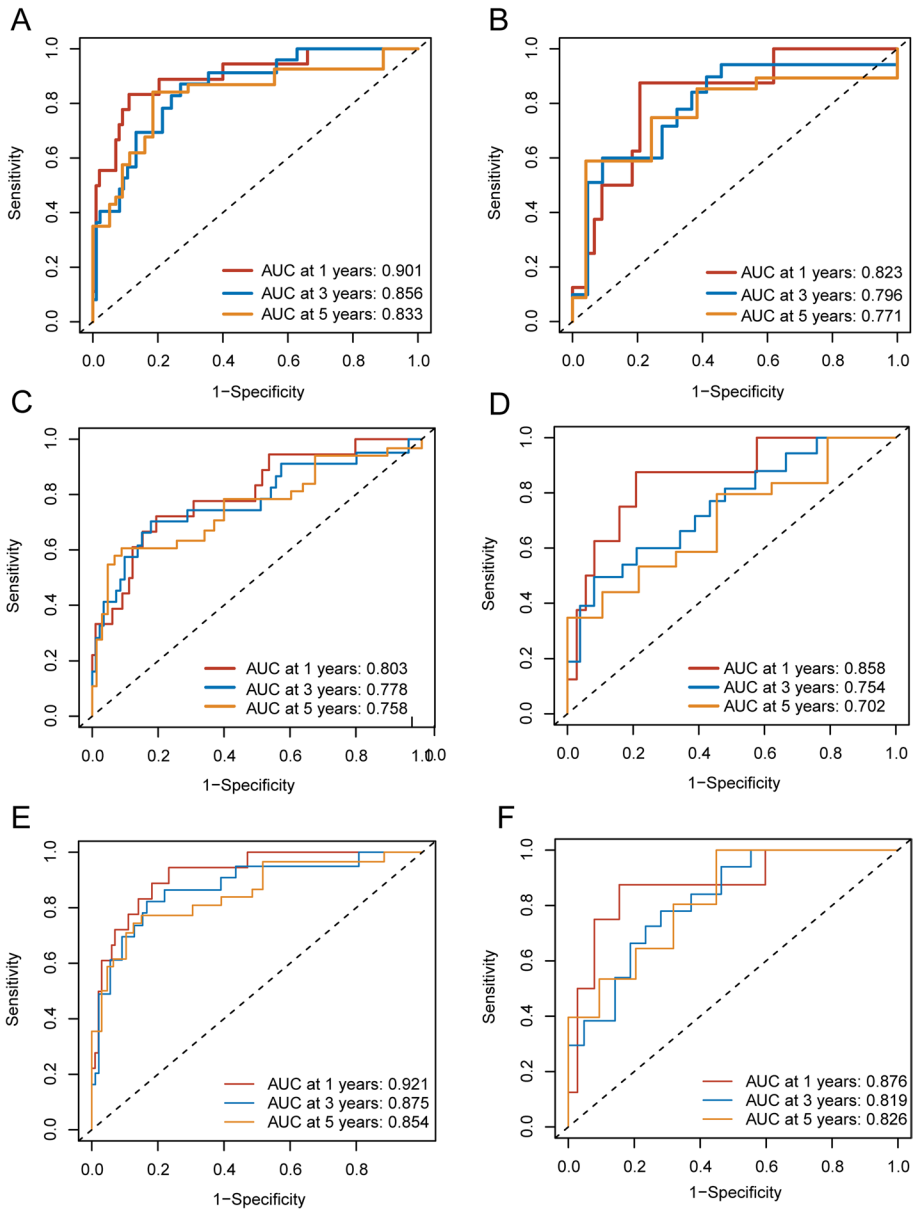

Fig. 4 ROC curve analyses of one-year, three-years, five-years for bRFS of three radiomics models. **A** periprostatic fat radiomics model in the training group. **B** periprostatic fat radiomics model in the validation group. **C** intratumoral radiomics model in the training group. **D** intratumoral radiomics model in the validation group. I periprostatic fat-intratumoral radiomics model in the training group. **F** periprostatic fat-intratumoral radiomics model in the validation group. ROC, the receiver operating characteristic. bRFS, biochemical recurrence-free survival

the periprostatic fat radiomics features with intratumoral radiomics features, the periprostatic fat-intratumoral radiomics score exhibited superior performance in predicting bRFS compared to the intratumoral radiomics score alone. Furthermore, the combined radiomics-clinical nomogram exhibited a high predictive performance to estimate bRFS of PCa patients after RP treatment.

Establishing an assessment model for bRFS in PCa patients is crucial for guiding treatment plans, influencing follow-up schedules, and enabling adjuvant therapy decisions. Firstly, by accurately stratifying patients based on their risk of BCR, the nomogram could guide clinicians in tailoring post-surgical treatment strategies. For instance, high-risk patients identified through the nomogram may benefit from closer monitoring or early initiation of adjuvant therapies such as ADT or radiotherapy, potentially improving long-term outcomes by catching recurrences earlier. This targeted approach can lead

Table 3 Comparing ROC curves of three radiomics scores

Radiomics scores	Training group ($n=118$)			Validation group ($n=53$)		
	AUC (95% CI)		*P* value	AUC (95% CI)		*P* value
1-Years bRFS						
Periprostatic fat-intratumoral vs. Intratumoral	0.921 (0.857–0.981)	0.803 (0.640–0.889)	0.010	0.876 (0.764–0.980)	0.858 (0.731–0.961)	0.467
Periprostatic fat-intratumoral vs. Periprostatic fat	0.921 (0.857–0.981)	0.901 (0.817–0.982)	0.413	0.876 (0.764–0.980)	0.823 (0.663–0.965	0.478
Periprostatic fat vs. Intratumoral	0.901 (0.817–0.982)	0.803 (0.640–0.889)	0.051	0.823 (0.663–0.965)	0.858 (0.731–0.961)	0.595
3-Years bRFS						
Periprostatic fat-intratumoral vs. Intratumoral	0.875 (0.763–0.950)	0.778 (0.606–0.865)	0.017	0.819 (0.696–0.931)	0.754 (0.624–0.895)	0.073
Periprostatic fat-intratumoral vs. Periprostatic fat	0.875 (0.763–0.950)	0.856 (0.741–0.923)	0.359	0.819 (0.696–0.931)	0.796 (0.656–0.943)	0.768
Periprostatic fat vs. Intratumoral	0.856 (0.741–0.923)	0.778 (0.606–0.865)	0.136	0.796 (0.656–0.943)	0.754 (0.624–0.895)	0.533
5-Years bRFS						
Periprostatic fat-intratumoral vs. Intratumoral	0.854 (0.706–0.923)	0.758 (0.600–0.827)	0.062	0.826 (0.710–0.935)	0.702 (0.610–0.863)	0.021
Periprostatic fat-intratumoral vs. Periprostatic fat	0.854 (0.706–0.923)	0.833 (0.687–0.921)	0.787	0.826 (0.710–0.935)	0.771 (0.642–0.905)	0.273
Periprostatic fat vs. Intratumoral	0.833 (0.687–0.921)	0.758 (0.600–0.827)	0.214	0.771 (0.642–0.905)	0.702 (0.610–0.863)	0.867

ROC Receiver operating characteristic, *bRFS* biochemical recurrence-free survival, *AUC* Area Under Curve, *CI* Confidence interval

Table 4 Univariate and multivariate Cox regression analyses exploring prognostic factors for predicting bRFS in patients with non-metastatic PCa receiving RP treatment

Variables	Univariate		Multivariate	
	HR (95% CI)	*P* value	HR (95% CI)	*P* value
Age at diagnosis	1.017 (0.961–1.076)	0.549	-	-
BMI	0.931 (0.825–1.050)	0.244	-	-
Initial PSA at diagnosis	1.024 (1.007–1.042)	0.005	1.017 (0.997–1.039)	0.102
Pathological T stage	2.780 (1.438–5.374)	0.002	3.006 (1.527–5.918)	0.001
ISUP grading group of surgical specimens	3.466 (1.699–7.069)	< 0.001	3.575 (1.700–7.519)	< 0.001
Positive surgical margin	4.401 (2.215–8.744)	< 0.001	3.96 (1.950–8.062)	< 0.001
Lymph nodes metastasis	1.005 (0.355–2.847)	0.992	-	-

bRFS biochemical recurrence-free survival, *PCa* Prostate cancer, *RP* radical prostatectomy, *HR* Hazard ratio, *CI* Confidence interval, *BMI* Body mass index, *PSA* Prostate-specific antigen, *ISUP* International Society of Urological Pathology

to more personalized and effective treatment pathways, maximizing the benefit of additional therapies in patients most likely to experience recurrence. Secondly, the nomogram could also significantly influence follow-up schedules. Patients with a higher predicted risk of recurrence might require more frequent PSA monitoring, imaging, and clinical assessments, enabling timely interventions if necessary. Conversely, patients with a lower predicted risk could follow standard or less intensive follow-up protocols, thereby reducing unnecessary hospital visits, medical costs, and patient anxiety. This stratified follow-up strategy could enhance resource allocation, allowing healthcare systems to focus efforts on high-risk patients while minimizing the burden on low-risk individuals. Thirdly, the predictive power of the nomogram may help in making informed decisions regarding the need for adjuvant therapies. For example, patients identified as high-risk may be recommended for early initiation of ADT or radiotherapy post-prostatectomy, which could play a pivotal role in preventing disease progression and improving long-term survival rates. On the other hand, low-risk patients might be spared from unnecessary adjuvant treatments, reducing their exposure to the associated side effects and preserving their quality of life. This individualized approach underscores the value of a radiomics-clinical model in supporting shared decision-making between patients and clinicians.

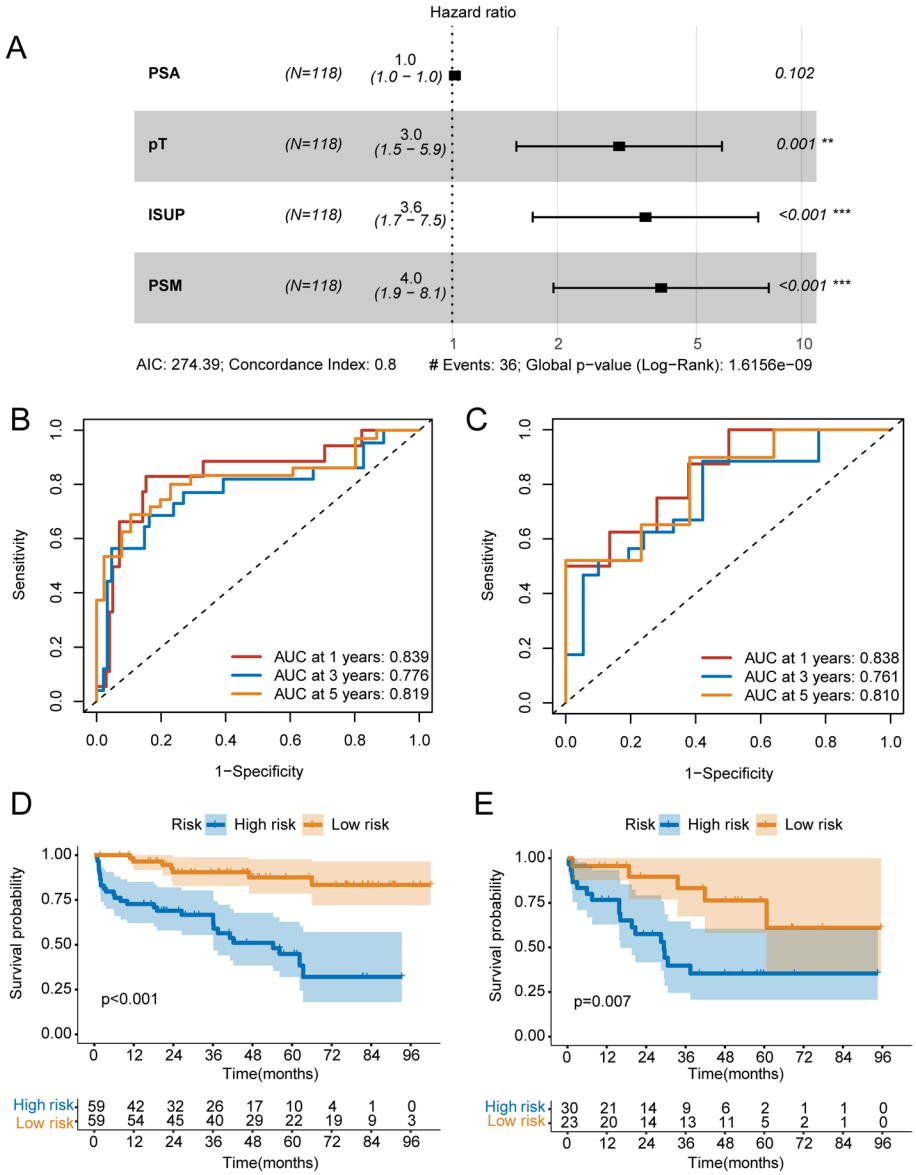

Fig. 5 Construction and validation of clinical model. **A** multivariate Cox regression analysis of clinical characteristics based on univariable Cox regression analysis. **B** ROC curve analyses of one-year, three-years, five-years for bRFS of clinical model in the training group. **C** ROC curve analyses of one-year, three-years, five-years for bRFS of clinical model in the validation group. **D** Kaplan-Meier curve analyses of clinical model in the training group. I Kaplan-Meier curve analyses of clinical model in the validation group. ROC, the receiver operating characteristic. bRFS, biochemical recurrence-free survival

Previous studies have provided evidence of the potential of radiomics features derived from MRI to estimate BCR in PCa patients following initial treatment. For instance, Shiradkar et al. demonstrated the utility of radiomics features derived from ADC and T2WI MRI in predicting BCR of PCa patients receiving RP [19]. Shahait et al. proposed a prediction model that integrates radiomic features extracted from MRI and other clinicopathological parameters for post-surgical bRFS; which performed better than other traditional models such as Decipher and CAPRA [20–22]. Bourbonne et al. developed an MRI-derived radiomics classifier that effectively predicted BCR among patients with PCa underwent RP, which was successfully validated and achieved an accuracy of 0.76 [23, 24]. However, these studies only extracted and modeled radiomics features within the intratumoral region. In our study, we simultaneously evaluated the predictive value of radiomics

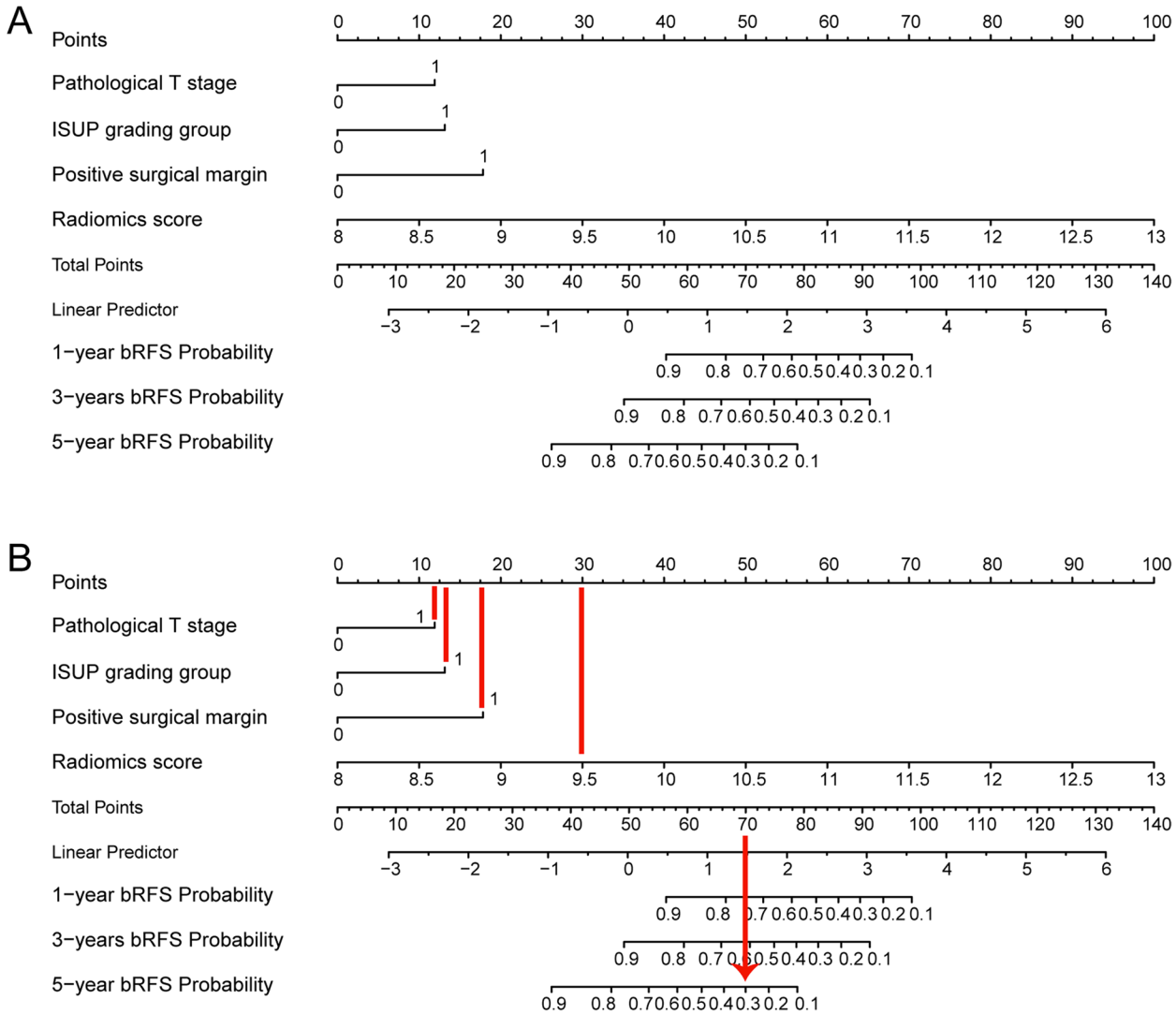

Fig. 6 The radiomics-clinical nomogram. **A** Nomogram for predicting one-year, three-years, five-years bRFS of PCa patients receiving RP treatment. **B** How to use: (1) locate the patient's radiomic score, Pathological T stage, ISUP grading group, Positivity surgical margin and then draw a straight line on the top dot axis to obtain the corresponding score; (2) sum the scores obtained; (3) find the final sum on the total point axis and draw a straight line down to assess the risk of bRFS in patients with PCa. bRFS, biochemical recurrence-free survival. PCa, prostate cancer

features derived from intratumoral and periprostatic fat region for predicting bRFS. ROC curve analysis revealed a strong relationship between intratumoral region radiomic features and bRFS, which was consistent with previous research. Furthermore, we observed a noteworthy finding that the AUCs of both periprostatic fat and intratumoral radiomics features were significantly increased, indicating a substantial improvement in the predictive efficiency by adding periprostatic fat radiomic features. Additionally, the construction of a nomogram combining radiomic features of the periprostatic fat and intratumoral region, along with clinicopathological features, achieved the highest AUC value. These findings underscore the significance of periprostatic fat radiomics in assessing tumor recurrence in clinical practice.

In recent years, researchers have observed features in the adipose tissue surrounding tumors that are linked to tumor progression, and these features can be captured and analyzed by radiomics methods. For example, Jayaprakasam et al. investigated the association between MRI radiomics features of mesorectal fat and clinical outcomes in patients with locally advanced rectal cancer. Their findings revealed that radiomics features derived from mesorectal fat exhibited predictive capabilities for various clinical parameters, including local and distant recurrence, pathological complete

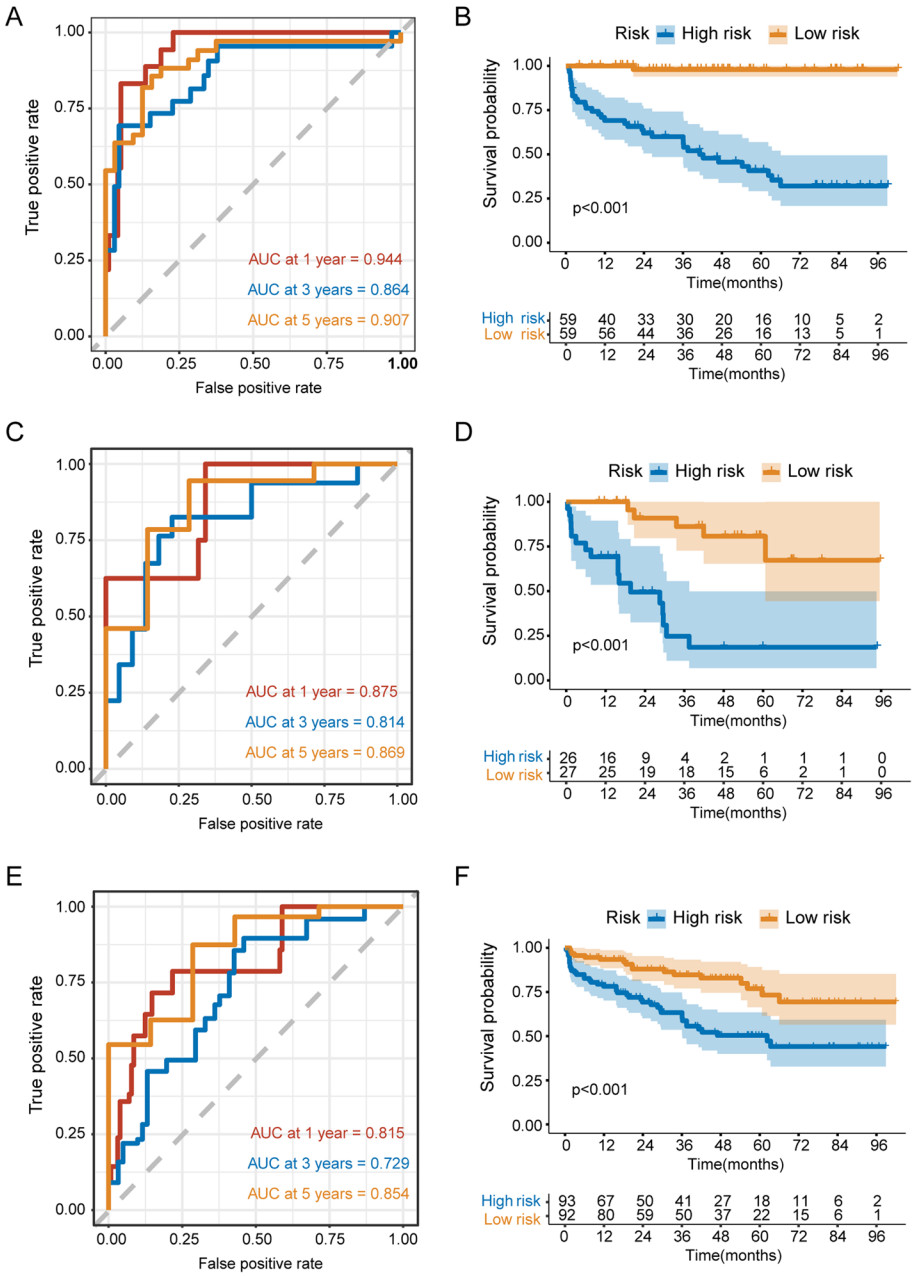

Fig. 7 ROC curve and Kaplan-Meier curve analyses of the radiomics-clinical nomogram. ROC curve analyses of one-year, three-years, five-years for bRFS of combined radiomics-clinical nomogram in the training group (**A**), validation group (**C**), and testing group I. Kaplan-Meier curve analyses of radiomics-clinical nomogram in the training group (**B**), validation group (**D**), and testing group (**F**). ROC, the receiver operating characteristic. bRFS, biochemical recurrence-free survival. PCa, prostate cancer. RP, radical prostatectomy

response, as well as post-treatment T and N categories in patients with locally advanced rectal cancer [25]. Ahn et al. discovered that radiomics features extracted from perigastric adipose tissue on 2-deoxy-2-[18 F] fluoro-D-glucose PET/CT ([18 F] FDG PET/CT) were substantial prognostic indicators for predicting recurrence-free survival among patients with gastric cancer [26]. Shaish et al. conducted a study investigating the potential value of pretreatment MRI-based radiomics extracted from locally advanced rectal cancer and the surrounding mesorectal compartment in predicting significant clinical outcomes. The optimal predictive performance was observed when utilizing the mesorectal compartment for predicting pathological

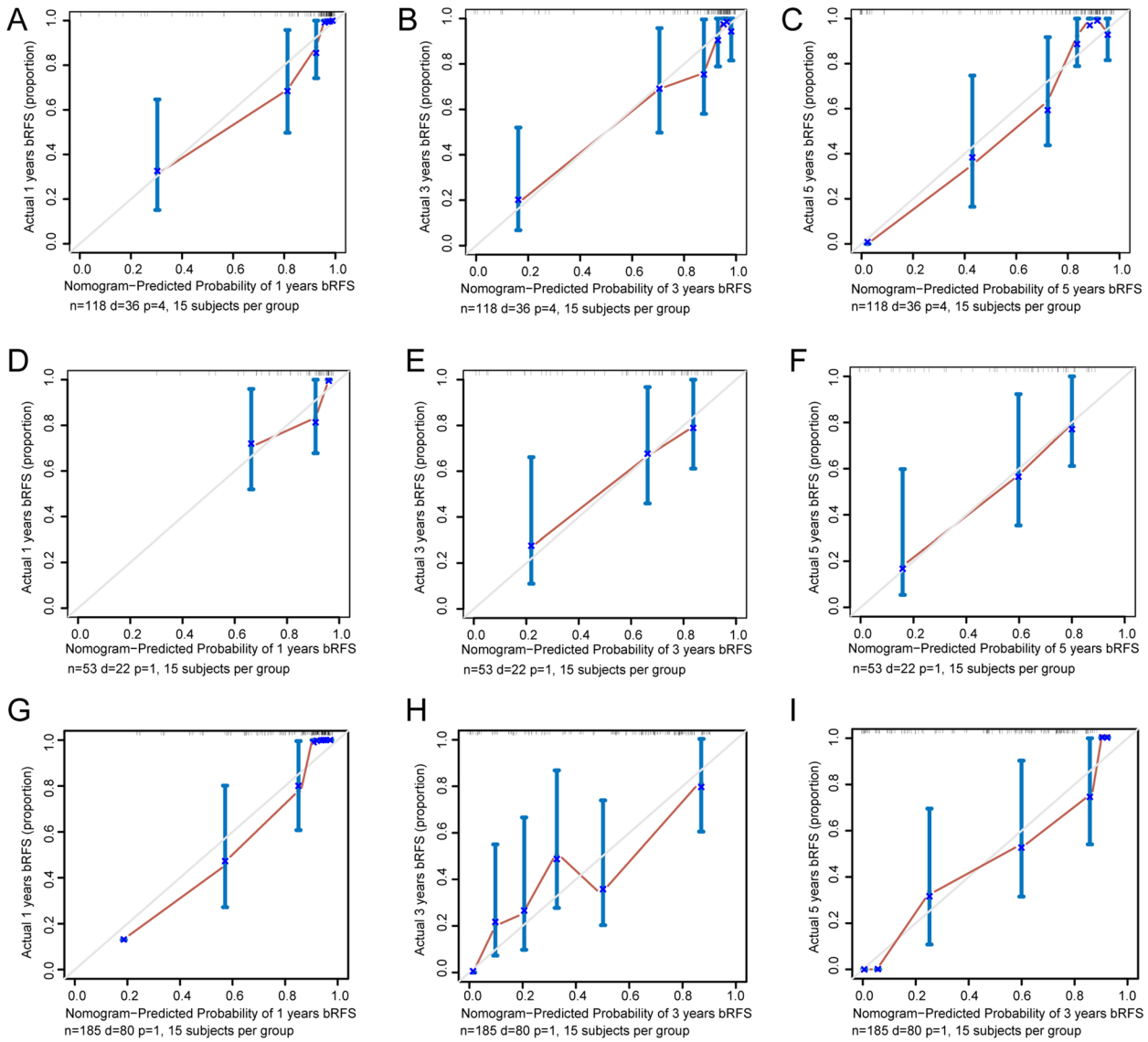

Fig. 8 Calibration curves of the combined radiomics-clinical nomogram. **A**-**C** Calibration curves of the combined radiomics-clinical nomogram for one-year, three-years, five-years bRFS in the training group. **D**-**F** Calibration curves of the combined radiomics-clinical nomogram for one-year, three-years, five-years bRFS in the validation group. **G**-**I** Calibration curves of the combined radiomics-clinical nomogram for one-year, three-years, five-years bRFS in the validation group. bRFS, biochemical recurrence-free survival

complete response and when employing a combined approach that leveraged both the mesorectal compartment and tumor region to predict tumor regression grade and neoadjuvant rectal score [27]. In our study, periprostatic fat radiomics model and intratumoral radiomics model demonstrated similar performance, and combined periprostatic fat-intratumoral radiomics features were more prognostic of bRFS compared to intratumoral radiomics features. These research findings suggested that the radiomics features of the peritumoral adipose tissue contain important prognostic information.

Periprostatic fat radiomics features could reflect the different biological characteristics, metabolic activity, and pathological features of the periprostatic fat tissue [28, 29]. The predictive ability of these radiomics features in relation to bRFS of PCa may be attributed to various factors. First, one reason for this predictive ability may be the detection of microscopic characteristic changes in periprostatic fat that are not visible to the naked eye

Table 5 Comparing ROC curves of optimal radiomics model, clinical model and radiomics-clinical nomogram

Predictive models	Training group ($n=118$)			Validation group ($n=53$)			Testing group ($n=185$)		
	AUC (95% CI)		*P* value	AUC (95% CI)		*P* value	AUC (95% CI)		*P* value
1-Years bRFS									
Nomogram vs. Radiomics model	0.944 (0.912–0.990)	0.921 (0.857–0.981)	0.329	0.875 (0.750–0.998)	0.876 (0.744–0.978)	0.915	0.815 (0.664–0.921)	0.807 (0.623–0.911)	0.201
Nomogram vs. Clinical model	0.944 (0.912–0.990)	0.839 (0.661–0.928)	0.009	0.875 (0.750–0.998)	0.838 (0.685–0.980)	0.402	0.815 (0.664–0.921)	0.779 (0.615–0.893)	0.553
Radiomics model vs. Clinical model	0.921(0.857–0.981)	0.839 (0.661–0.928)	0.123	0.876 (0.744–0.978)	0.838 (0.685–0.980)	0.616	0.807 (0.623–0.911)	0.779 (0.615–0.893)	0.679
3-Years bRFS									
Nomogram vs. Radiomics model	0.864 (0.772–0.969)	0.875 (0.762–0.949)	0.705	0.814 (0.676–0.953)	0.819 (0.696–0.945)	0.897	0.729 (0.641–0.883)	0.714 (0.626–0.842)	0.424
Nomogram vs. Clinical model	0.864 (0.772–0.969)	0.776 (0.602–0.872)	0.008	0.814 (0.676–0.953)	0.761 (0.616–0.914)	0.241	0.729 (0.641–0.883)	0.703 (0.605–0.847)	0.386
Radiomics model vs. Clinical model	0.875 (0.762–0.949)	0.776 (0.602–0.872)	0.115	0.819 (0.696–0.945)	0.761 (0.616–0.914)	0.477	0.714 (0.626–0.842)	0.703 (0.605–0.847)	0.553
5-Years bRFS									
Nomogram vs. Radiomics model	0.907 (0.836–0.982)	0.854 (0.706–0.923)	0.050	0.869 (0.712–0.997)	0.826 (0.630–0.997)	0.142	0.854 (0.702–0.913)	0.817 (0.712–0.955)	0.658
Nomogram vs. Clinical model	0.907 (0.836–0.982)	0.819 (0.687–0.915)	0.027	0.869 (0.712–0.997)	0.810 (0.689–0.998)	0.721	0.854 (0.702–0.913)	0.805 (0.704–0.942)	0.349
Radiomics model vs. Clinical model	0.854 (0.706–0.923)	0.819 (0.687–0.915)	0.876	0.826 (0.630–0.997)	0.810 (0.689–0.998)	0.448	0.817 (0.712–0.955)	0.805 (0.704–0.942)	0.695

ROC Receiver operating characteristic, *bRFS* biochemical recurrence-free survival, *AUC* Area Under Curve, *CI* Confidence interval

but that play a vital role in tumor development. Abd Elmageed et al. demonstrated that PCa triggers protumorigenesis in periprostatic adipose tissue. Their findings unveiled that the medium utilized for culturing PCa cells triggered tumor-like alterations in preadipocytes, encompassing epithelial-mesenchymal transition, genetic variability, and the formation of tumor-like lesion in vivo [30]. These results propose that a persistent positive feedback loop between PCa and the periprostatic environment hastens the progressive deterioration of the disease. Second, the structure and metabolic level of periprostatic adipose tissue have been found to be associated with the growth and spread of PCa [31, 32]. Studies have demonstrated that PCa cells can derive nutrients and energy from periprostatic adipose tissue, promoting tumor growth and metastasis [16, 33, 34]. Coy et al. reported that lipid metabolism disturbances in periprostatic adipose tissue can influence tumor cell processes by inducing metabolic changes [17]. Laurent et al. [35]. shown that the uptake of exogenous lipids promotes tumor cell invasion. These transferred lipids stimulate the expression of one isoform of the pro-oxidant enzyme NADPH oxidase, NOX5. NOX5 increases intracellular reactive oxygen species (ROS), which in turn activate the HIF1/MMP14 pathway, leading to enhanced tumor cell invasion. Gang Liu et al. [36]. reported that prostate-specific expression of the IL-6 transgene has been shown to autonomously induce prostate neoplasm by amplifying inflammation within both the prostate and periprostatic adipose tissue. The identification of radiomics features reflecting the structure and metabolic changes in periprostatic adipose tissue has been instrumental in predicting tumor recurrence. Third, PCa cells may persist in the periprostatic fat tissue following RP or radiotherapy [37]. A thorough analysis of periprostatic tissue radiomics features allows for a more accurate identification of residual cancer foci or lymph node metastasis [38, 39], ultimately improving BCR prediction performance.

This study exhibited several limitations. Firstly, it was a retrospective investigation conducted at a single center, featuring a restricted sample size. Additionally, the nomogram constructed in this study was only internally

validated and lacked external validation. It is essential to conduct prospective validation studies in multicenter and large-scale cohorts to confirm these findings. Secondly, manual delineation of the ROI inevitably introduces some degree of variability. To address this, we implemented several measures to minimize bias and enhance the accuracy of ROI delineation. The ROIs were carefully marked by two experienced radiologists with extensive training in prostate MRI. Inter-observer and intra-observer repeatability were quantified by employing the infraclass correlation coefficient (ICC). Features with ICC greater than 0.8 were chosen for further analysis. Thirdly, there is a significant difference in the distribution of pathological T stage between the training and validation cohorts. This difference in T stage distribution may potentially likely impacted the model's performance. This imbalance in pathological T stage distribution between the training and validation cohorts might potentially likely impacted the model's performance. The model, having been trained on a cohort with a more balanced pathological T stage distribution, may have been less effective in a population where advanced T stage predominated, as the clinical parameters associated with advanced pathological T stage could potentially overshadow the contributions of the other variables included in the nomogram.

Conclusions

The study found that the combined periprostatic fat-intratumoral radiomics features were more prognostic of bRFS compared to intratumoral radiomics features. The combined radiomics-clinical nomogram exhibited a high predictive performance to estimate bRFS of PCa patients after RP treatment. This study underlined that radiomic features of periprostatic adipose tissue could provide more comprehensive and accurate information on PCa lesions.

Abbreviations

mpMRI	Multiparametric magnetic resonance imaging
bRFS	Biochemical recurrence-free survival
PCa	Prostate cancer
RP	Receiving radical prostatectomy
LASSO	Least absolute shrinkage and selection operator
ROC	Receiver operating characteristic
AUC	Area Under the Curve
CI	Confidence interval
BCR	Biochemical recurrence
TNF	Tumor necrosis factor
CCL7	C-C motif chemokine ligand 7
AJCC/UICC	American Joint Committee on Cancer/ Union for International Cancer Control
TNM	Tumor, Node, Metastasis
T2WI	T2 weighted images
ADC	Apparent Diffusion Coefficient
PSA	Prostate specific antigen
EAU	European Association of Urology
ROI	Regions of interest
LoG	Laplacian of Gaussian
GLRLM	gray-level run length matrix
GLCM	gray-level co-occurrence matrix
GLDM	gray-level dependence matrix
GLSZM	gray-level size zone matrix
NGTDM	neighboring gray tone difference matrix
ICC	Infraclass correlation coefficient
[18F] FDG PET/CT	2-deoxy-2-[18 F] fluoro-D-glucose positron emission tomography/computed tomography

Supplementary Information

The online version contains supplementary material available at https://doi.org/10.1186/s12885-024-13207-4.

Supplementary Material 1: Supplementary Figure 1. Schematic diagram of the periprostatic fat ROI outline in the MRI images of PCa patient. (A) is the T2WI sequence with PCa in the periprostatic fat region. (B) is the ADC sequence with PCa in the periprostatic fat region. (C) is the periprostatic fat ROI outline in the T2WI sequence. (D) is the periprostatic fat ROI outline in the ADC sequence. (E) is the generated periprostatic fat ROI in the T2WI sequence. (F) is the generated periprostatic fat ROI in the ADC sequence. ROI, regions of interest; MRI, magnetic resonance imaging; PCa, prostate cancer; T2WI, T2-weighted imaging; ADC, apparent-diffusion coefficient.

Supplementary Material 2: Supplementary Figure 2. Schematic diagram of the intratumoral ROI outline in the MRI images of PCa patient. (A) is the T2WI sequence in the intratumoral region. (B) is the ADC sequence in the intratumoral region. (C) is the intratumoral ROI outline in the T2WI sequence. (D) is the intratumoral ROI outline in the ADC sequence. (E) is the generated intratumoral ROI in the T2WI sequence. (F) is the generated intratumoral ROI in the ADC sequence. ROI, regions of interest; MRI, magnetic resonance imaging; PCa, prostate cancer; T2WI, T2-weighted imaging; ADC, apparent-diffusion coefficient.

Supplementary Material 3.

Supplementary Material 4.

Supplementary Material 5.

Acknowledgements

Not applicable.

Authors' contributions

Writing – original draft, Xiao-Hui Wu, Zhi-Bin Ke, Ze-Jia Chen, Wen-Qi Liu. Writing – review & editing, Yong Wei, Ning Xu. Methodology, Shao-Hao Chen, Dong-Ning Chen. Formal analysis, Qing-Shui Zheng, Shao-Hao Chen, Yu-Ting Xue. Data curation, Shao-Hao Chen, Xue-Yi Xue. Conceptualization, Yong Wei, Xue-Yi Xue. Visualization, Yong Wei. Project administration, Yong Wei, Ning Xu.

Funding

This work was supported by Science and Technology Innovation Joint Fund project of Fujian province (No. 2021Y9126); Science and Technology Innovation Joint Fund project of Fujian province (No. 2023Y9078); Natural Science Foundation of Fujian Province (No. 2024J01556).

Data availability

The datasets used and/or analyzed during the current study are available from the corresponding author on reasonable request.

Declarations

Ethics approval and consent to participate

This study was approved by the Ethics Committee of the First Affiliated Hospital of Fujian Medical University (Approved No. of ethic committee: MRCTA, ECFAH of FMU [2024]638), and all patients provided written informed consent.

Consent for publication

Not applicable.

Competing interests
The authors declare no competing interests.

Author details
[1]Department of Urology, Urology Research Institute, the First Affiliated Hospital, Fujian Medical University, Fuzhou 350005, China. [2]Department of Urology, Binhai Campus of the First Affiliated Hospital, National Region Medical centre, Fujian Medical University, Fuzhou 350212, China. [3]Fujian Key Laboratory of Precision Medicine for Cancer, the First Affiliated Hospital, Fujian Medical University, Fuzhou 350005, China.

Received: 2 February 2024 Accepted: 15 November 2024
Published online: 27 November 2024

References

1. Sung H, Ferlay J, Siegel RL, Laversanne M, Soerjomataram I, Jemal A, et al. Global Cancer statistics 2020: GLOBOCAN estimates of incidence and mortality worldwide for 36 cancers in 185 countries. Cancer J Clin. 2021;71(3):209–49.
2. Litwin MS, Tan H-J. The diagnosis and treatment of prostate cancer: a review. JAMA. 2017;317(24):2532–42.
3. Van den Broeck T, van den Bergh RCN, Arfi N, Gross T, Moris L, Briers E, et al. Prognostic value of biochemical recurrence following treatment with curative intent for prostate cancer: a systematic review. Eur Urol. 2019;75(6):967–87.
4. Freedland SJ, Humphreys EB, Mangold LA, Eisenberger M, Dorey FJ, Walsh PC, et al. Risk of prostate cancer-specific mortality following biochemical recurrence after radical prostatectomy. JAMA. 2005;294(4):433–9.
5. Lambin P, Leijenaar RTH, Deist TM, Peerlings J, de Jong EEC, van Timmeren J, et al. Radiomics: the bridge between medical imaging and personalized medicine. Nat Rev Clin Oncol. 2017;14(12):749–62.
6. Bera K, Braman N, Gupta A, Velcheti V, Madabhushi A. Predicting cancer outcomes with radiomics and artificial intelligence in radiology. Nat Rev Clin Oncol. 2022;19(2):132–46.
7. Spohn SKB, Bettermann AS, Bamberg F, Benndorf M, Mix M, Nicolay NH, et al. Radiomics in prostate cancer imaging for a personalized treatment approach - current aspects of methodology and a systematic review on validated studies. Theranostics. 2021;11(16):8027–42.
8. Ghezzo S, Bezzi C, Presotto L, Mapelli P, Bettinardi V, Savi A, et al. State of the art of radiomic analysis in the clinical management of prostate cancer: a systematic review. Crit Rev Oncol Hematol. 2022;169:103544.
9. Woźnicki P, Westhoff N, Huber T, Riffel P, Froelich MF, Gresser E, et al. Multiparametric MRI for prostate cancer characterization: combined use of radiomics model with PI-RADS and clinical parameters. Cancers (Basel). 2020;12(7):1767.
10. Wang Y, Yu B, Zhong F, Guo Q, Li K, Hou Y, et al. MRI-based texture analysis of the primary tumor for pre-treatment prediction of bone metastases in prostate cancer. Magn Reson Imaging. 2019;60:76–84.
11. Abdollahi H, Mahdavi SR, Mofid B, Bakhshandeh M, Razzaghdoust A, Saadipoor A, et al. Rectal wall MRI radiomics in prostate cancer patients: prediction of and correlation with early rectal toxicity. Int J Radiat Biol. 2018;94(9):829–37.
12. Abdollahi H, Mofid B, Shiri I, Razzaghdoust A, Saadipoor A, Mahdavi A, et al. Machine learning-based radiomic models to predict intensity-modulated radiation therapy response, Gleason score and stage in prostate cancer. Radiol Med. 2019;124(6):555–67.
13. Gregg JR, Surasi DS, Childs A, Moll N, Ward JF, Kim J, et al. The association of periprostatic fat and grade group progression in men with localized prostate cancer on active surveillance. J Urol. 2021;205(1):122–8.
14. Salji M, Hendry J, Patel A, Ahmad I, Nixon C, Leung HY. Peri-prostatic fat volume measurement as a predictive tool for castration resistance in advanced prostate cancer. Eur Urol Focus. 2018;4(6):858–66.
15. Li Y, Wu Y, Huang M, Zhang Y, Bai Z. Automatic prostate and peri-prostatic fat segmentation based on pyramid mechanism fusion network for T2-weighted MRI. Comput Methods Programs Biomed. 2022;223:106918.
16. Fontaine A, Bellanger D, Guibon R, Bruyère F, Brisson L, Fromont G. Lipophagy and prostate cancer: association with disease aggressiveness and proximity to periprostatic adipose tissue. J Pathol. 2021;255(2):166–76.
17. Altuna-Coy A, Ruiz-Plazas X, Sánchez-Martin S, Ascaso-Til H, Prados-Saavedra M, Alves-Santiago M, et al. The lipidomic profile of the tumoral periprostatic adipose tissue reveals alterations in tumor cell's metabolic crosstalk. BMC Med. 2022;20(1):255.
18. Kimura S, Urabe F, Sasaki H, Kimura T, Miki K, Egawa S. Prognostic significance of prostate-specific antigen persistence after radical prostatectomy: a systematic review and meta-analysis. Cancers (Basel). 2021;13(5):948.
19. Shiradkar R, Ghose S, Jambor I, Taimen P, Ettala O, Purysko AS, et al. Radiomic features from pretreatment biparametric MRI predict prostate cancer biochemical recurrence: preliminary findings. J Magn Reson Imaging. 2018;48(6):1626–36.
20. Li L, Shiradkar R, Leo P, Algohary A, Fu P, Tirumani SH, et al. A novel imaging based Nomogram for predicting post-surgical biochemical recurrence and adverse pathology of prostate cancer from pre-operative bi-parametric MRI. EBioMedicine. 2021;63:103163.
21. Brajtbord JS, Leapman MS, Cooperberg MR. The CAPRA score at 10 years: contemporary perspectives and analysis of supporting studies. Eur Urol. 2017;71(5):705–9.
22. Ross AE, Johnson MH, Yousefi K, Davicioni E, Netto GJ, Marchionni L, et al. Tissue-based Genomics augments post-prostatectomy risk stratification in a natural history cohort of Intermediate- and high-risk men. Eur Urol. 2016;69(1):157–65.
23. Bourbonne V, Fournier G, Vallières M, Lucia F, Doucet L, Tissot V et al. External validation of an MRI-Derived Radiomics Model to predict biochemical recurrence after surgery for high-risk prostate Cancer. Cancers (Basel). 2020;12(4):814.
24. Bourbonne V, Vallières M, Lucia F, Doucet L, Visvikis D, Tissot V, et al. MRI-derived radiomics to guide post-operative management for high-risk prostate cancer. Front Oncol. 2019;9:807.
25. Jayaprakasam VS, Paroder V, Gibbs P, Bajwa R, Gangai N, Sosa RE, et al. MRI radiomics features of mesorectal fat can predict response to neoadjuvant chemoradiation therapy and tumor recurrence in patients with locally advanced rectal cancer. Eur Radiol. 2022;32(2):971–80.
26. Ahn H, Song GJ, Jang S-H, Son MW, Lee HJ, Lee M-S, et al. Predicting the recurrence of gastric cancer using the textural features of perigastric adipose tissue on [18F]FDG PET/CT. Int J Mol Sci. 2022;23(19):11985.
27. Shaish H, Aukerman A, Vanguri R, Spinelli A, Armenta P, Jambawalikar S, et al. Radiomics of MRI for pretreatment prediction of pathologic complete response, tumor regression grade, and neoadjuvant rectal score in patients with locally advanced rectal cancer undergoing neoadjuvant chemoradiation: an international multicenter study. Eur Radiol. 2020;30(11):6263–73.
28. Liu D, Chen J, Ge H, Yan Z, Luo B, Hu X, et al. Radiogenomics to characterize the immune-related prognostic signature associated with biological functions in glioblastoma. Eur Radiol. 2023;33(1):209–20.
29. Zheng H, Miao Q, Liu Y, Mirak SA, Hosseiny M, Scalzo F, et al. Multiparametric MRI-based radiomics model to predict pelvic lymph node invasion for patients with prostate cancer. Eur Radiol. 2022;32(8):5688–99.
30. Abd Elmageed ZY, Yang Y, Thomas R, Ranjan M, Mondal D, Moroz K, et al. Neoplastic reprogramming of patient-derived adipose stem cells by prostate cancer cell-associated exosomes. Stem Cells. 2014;32(4):983–97.
31. Toren P, Venkateswaran V. Periprostatic adipose tissue and prostate cancer progression: new insights into the tumor microenvironment. Clin Genitourin Cancer. 2014;12(1):21–6.
32. Cancel M, Pouillot W, Mahéo K, Fontaine A, Crottès D, Fromont G. Interplay between prostate cancer and adipose microenvironment: a complex and flexible scenario. Int J Mol Sci. 2022;23(18):10762.
33. Ribeiro R, Monteiro C, Cunha V, Oliveira MJ, Freitas M, Fraga A, et al. Human periprostatic adipose tissue promotes prostate cancer aggressiveness in vitro. J Exp Clin Cancer Res. 2012;31(1):32.
34. Figiel S, Pinault M, Domingo I, Guimaraes C, Guibon R, Besson P, et al. Fatty acid profile in peri-prostatic adipose tissue and prostate cancer aggressiveness in african-caribbean and caucasian patients. Eur J Cancer. 2018;91:107–15.
35. Laurent V, Toulet A, Attané C, Milhas D, Dauvillier S, Zaidi F, et al. Periprostatic adipose tissue favors prostate cancer cell invasion in an obesity-dependent manner: role of oxidative stress. Mol Cancer Res. 2019;17(3):821–35.
36. Liu G, Zhang J, Frey L, Gang X, Wu K, Liu Q, et al. Prostate-specific IL-6 transgene autonomously induce prostate neoplasm through amplifying

inflammation in the prostate and peri-prostatic adipose tissue. J Hematol Oncol. 2017;10(1):14.
37. Van den Broeck T, van den Bergh RCN, Briers E, Cornford P, Cumberbatch M, Tilki D, et al. Biochemical recurrence in prostate cancer: the uropean association of urology prostate cancer guidelines panel recommendations. Eur Urol Focus. 2020;6(2):231–4.
38. Kwon YS, Ha Y-S, Modi PK, Salmasi A, Parihar JS, Patel N, et al. Oncologic outcomes in men with metastasis to the prostatic anterior fat pad lymph nodes: a multi-institution international study. BMC Urol. 2015;15:79.
39. Korten M, Pose RM, Graefen M, Tilki D, Michl U, Knipper S, et al. Preprostatic lymph nodes in prostate cancer hot or not? Impact on oncological outcome after radical prostatectomy. World J Urol. 2022;40(9):2231–7.

Publisher's Note